JOURNAL OF PROPULSION AND POWER
Vol. 22, No. 3, May–June 2006

Characterization of Side-Dump Combustor Flowfield Using Particle Image Velocimetry

Kyubok Ahn* and Youngbin Yoon†
Seoul National University, Seoul 151-742, Korea

An experimental study was carried out to investigate the instantaneous flowfield in a side-dump combustor using particle image velocimetry and examine the systematic effects of geometric variations (inlet angle and dome height) on the mean flowfield and the recirculation zones. The instantaneous velocity fields showed that the recirculation zones in the combustor consisted of large-scale and small-scale vortices, and the flow pattern might change periodically due to the oscillation of two inlet jets. The mean velocity fields indicated that as the inlet angle increased, the height of the secondary recirculation zone and the maximum reverse mass flow rate at transport into the primary recirculation zone increased almost linearly. The results also indicated that there was an optimum dome height for each inlet angle even though the dome height did not significantly affect the flowfield downstream of the combustor inlet. The values of the maximum reverse mass flow rate in the secondary recirculation zone were equivalent to those in the primary recirculation zone, so the secondary recirculation zone was believed to be as important as the primary recirculation zone for flame stabilization.

Nomenclature

H	=	inner height of the combustor
H_{SRZ}	=	transverse height of the secondary recirculation zone
h_D	=	dome height
h_D^*	=	nondimensional dome height (normalized by H)
L	=	inner length of the combustor
L_{SRZ}	=	longitudinal length of the secondary recirculation zone
$\dot{m}_{\mathrm{in}}$	=	total inlet mass flow rate
$\dot{m}_{\mathrm{max,PRZ}}$	=	maximum reverse mass flow rate in the primary recirculation zone
$\dot{m}_{\mathrm{max,SRZ}}$	=	maximum reverse mass flow rate in the secondary recirculation zone
$\dot{m}_{\mathrm{PRZ}}$	=	reverse mass flow rate in the primary recirculation zone
$\dot{m}_{ri}$	=	mass flow rate transported into the dome region
U	=	longitudinal velocity
U_{ref}	=	reference velocity
V	=	transverse velocity
W	=	inner width of the combustor
X	=	combustor longitudinal coordinate
X^*	=	nondimensional combustor longitudinal coordinate (normalized by H)
Y	=	combustor transverse coordinate
Y^*	=	nondimensional combustor transverse coordinate (normalized by H)
θ	=	side inlet angle
ω_z	=	vorticity component normal to the measurement plane

Subscripts

PRZ	=	primary recirculation zone
SRZ	=	secondary recirculation zone
max	=	maximum

Received 17 December 2002; accepted for publication 13 September 2005.

*Graduate Student, Institute of Advanced Aerospace Technology, School of Mechanical and Aerospace Engineering, San 56-1, Shinlim-dong, Kwanak-ku.

†Associate Professor, Institute of Advanced Aerospace Technology, School of Mechanical and Aerospace Engineering, San 56-1, Shinlim-dong, Kwanak-ku; ybyoon@snu.ac.kr. Member AIAA.

I. Introduction

SUDDEN-EXPANSION-TYPE combustors have been studied for a long time as a basic configuration for an integrated rocket ramjet.[1–3] Because the velocity of the airflow in the combustor is in general higher than the flame propagation speed, it is necessary to have a flame holder for flame stabilization. Instead of employing conventional flame holders, combustors make use of recirculation zones, which are formed by sudden-expansion areas that act as flame stabilization regions. According to the inlet configurations, coaxial-dump or side-dump combustors have mostly been used.[4] For a side-dump combustor, it is generally known that a primary recirculation zone (PRZ) is generated between a dome and a combustor inlet, and a secondary recirculation zone (SRZ) is formed near the wall downstream of the combustor inlet.

Over the past decades, a number of researchers have investigated the flowfield in side-dump combustors. Stull et al.[5] showed the qualitative time-mean flow streamline patterns of a dual side-dump combustor, taking photographs of air bubbles in a water tunnel combustor model. They reported that the variations in dome heights greatly affected the flowfield in the dome, but had little influence on the flowfield downstream of the inlet ducts. Nosseir and Behar[6] and Nosseir et al.[7] studied the characteristics of jet impingement in a side-dump combustor and found that the strength and direction of rotation of the vortices generated by the impingement of two jets were phase-locked with the oscillations of the jets in and out of the dome.

Liou and Wu[8] and Liou et al.[9] investigated experimentally and numerically the flowfield characteristics in a side-dump combustor with two 60-deg curved inlets. They presented detailed quantitative profiles of mean velocities and turbulence intensities using laser Doppler velocimetry. Liou et al.[10] conducted numerical simulations with various turbulence models. With a varied inlet angle, Manjunath et al.[11,12] measured the effect of the mean flow and turbulence characteristics on the mixing of two nonaxial plane jets using pitot tubes and hot wires. They reported that the inlet angle considerably affected the extent of the recirculation zones and the rate of mixing of the two jets. Yen and Ko[13] numerically studied the effects of the side inlet angle on the flowfield in a three-dimensional side-dump combustor and found that the flowfield in a three-dimensional side-dump combustor was much different from that in a two-dimensional axisymmetric side-dump combustor due to the different flow space.

Although understanding the dynamics of these flows is important for designing the combustor and a number of studies have been

performed for that purpose, our knowledge and our experimental data on the flowfield remain incomplete. The main reasons are as follows: the limited literature available, the lack of instantaneous multidimensional quantitative measurement techniques, and the complexity of varying experimental configurations. Accordingly, experimental data with two-dimensional instantaneous velocities and two-dimensional mean velocities taking into account the systematic effects of the inlet angle and the dome height are in limited number.

Therefore, the present research was carried out to investigate the instantaneous flowfield in the side-dump combustor using a particle image velocimetry (PIV) technique, which can acquire instantaneous two-dimensional velocities with high spatial resolution, and examine the systematic effects of geometric variations (inlet angle and dome height) on the mean flowfield and the recirculation zones. The results of the study would help in understanding the flow structures and designing the ramjet combustor and would provide a quantitative database for numerical simulation researchers.

II. Experimental Apparatus and Condition

A. Experimental System and Particle Image Velocimetry System

Figure 1 shows the schematic of a side-dump combustor and a particle image velocimetry (PIV) system. The combustor system consists of a ring blower that produces air, a settling chamber for stabilizing air, an aerosol generator for flow visualization, and a two-dimensional shaped combustor with two symmetric inlets, which are located at an angle of 180 deg. For a direct connect test, a blower that could supply a maximum airflow of 8 m^3/min and a settling chamber with size $0.5 \times 0.5 \times 0.6$ m were used. This blower could be adjusted to give bulk velocities at up to 88 m/s in the combustor inlet. Most olive oil particles, which were produced by the PIV particle generator, were 0.5–1.5 μm in diameter and had a peak value at 1 μm diameter. The particles were transported into the settling chamber. Particle seeding density could be controlled by a regulator and valves, which were connected to pressurized air and Laskin nozzles. The stabilized air in the chamber was separated into two rectangular ducts to supply air into two symmetric inlets of the combustor. The airflow rate through the inlets was controlled precisely by valves and manometers, which were connected to rectangular ducts. The inner size of the rectangular ducts was $16 \times 46 \times 600$ mm.

The schematic of the PIV system setup is presented in Fig. 1. In the present experiment, two 532-nm laser beams (second harmonic beams of a Spectra Physics GCR-170 YAG laser) were used and changed to sheet beams through a set of cylindrical lenses. The energy of the laser beam per pulse was 30 mJ, and the duration of each pulse was 8 ns. The pulse separation between two laser beams was controlled by a delay generator (Stanford, DG535). The pulse separation was confirmed using a photodiode and was fixed to 20 μs throughout the experiments.

Scattered images from the seeding particles were recorded on a digital camera (Kodak Megaplus ES1.0, 1008 × 1018 pixels) equipped with an f/2.8 AF Micro Nikkor 105-mm lens. For synchronization with the laser pulses, the exposure time of the camera was also controlled using the delay generator. The velocity vectors were calculated by the fast Fourier transform-based cross-correlation technique. The resolution of an interrogation region was

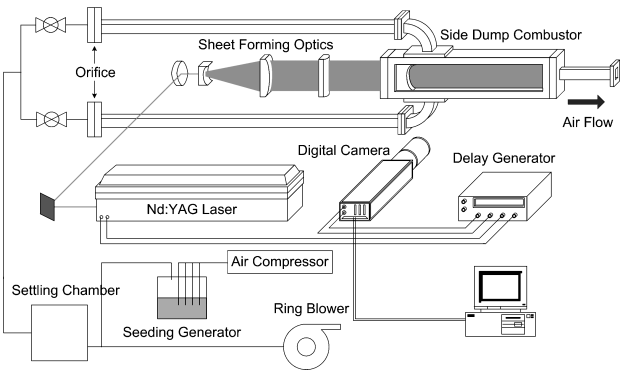

Fig. 1 Schematic of experimental system and PIV system.

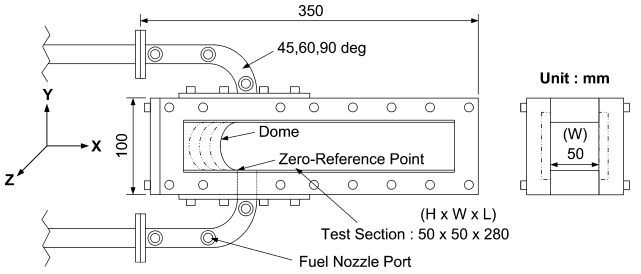

Fig. 2 Experimental setup of the model side-dump combustor.

32×32 pixels with a 50% overlap, which was equivalent to a spatial size of 1.37×1.37 mm. Therefore, the minimum vortex that could be properly visualized had a size of 4.1×4.1 mm because vectors with a 3×3 matrix were needed to calculate the vorticity. The correlation-based correction algorithm, which was proposed by Hart,[14] was used to improve the signal-to-noise ratio and remove error vectors.

B. Model Combustor and Experimental Condition

The model side-dump combustor is shown in Fig. 2. The dome height, which was defined as a length from the zero reference point to the center point of the dome, could be 12.5, 22.5, 32.5, or 42.5 mm. The dome was composed of two parts with a 2.0-mm vertical crevice in the centerline to enable the laser sheet beam to pass the dome and illuminate through the combustor. The inner size of the combustor was $50 \times 50 \times 280$ mm ($H \times W \times L$). A quartz window was built ahead of the dome to pass a laser sheet beam and to block air leakage. A visualization window was built into the front wall of the combustor for taking photographs of seeding particles. No exit nozzle was used in the present experiment. The combustor inlets were symmetric and their angles could be varied to 45, 60, and 90 deg. The combustor and rectangular ducts were mounted on a traversing device. This arrangement made it possible to move the combustor system along the X, Y, and Z directions to any desired location without realigning the PIV system setup.

Because the length of the combustor was much greater than the height, the recording area of the camera was selected as 8×8 cm. By moving the combustor 7 cm along the longitudinal direction using the traversing device, the flowfields in the combustor could be measured at three different locations. Hence, the flowfields were measured up to 18 cm downstream from the zero reference point. The air velocity in the combustor inlet was fixed to 40 m/s, which was used as a reference velocity (U_{ref}) to normalize the experimental results. The height of the combustor was used as a reference length. The Reynolds number based on the combustor height was 8.8×10^4, indicating that the flow was turbulent.

III. Results and Discussion

A. Instantaneous Velocity Characteristics

The instantaneous two-dimensional velocities in the combustor were obtained for all three inlet angles and four dome heights. Figure 3 presents those velocities in three different cases. In all cases, a pair of counter-rotating vortices are shown ahead of the impinging point. The centers of the counter-rotating vortices are plotted as solid circles. The pair of counter-rotating vortices was driven by sudden expansion of the inlet flow, by shear force of the jet, and by spread-out flow of the jet impinging.[8] Unlike the result of the mean flowfield reported by Manjunath et al.,[11] the vortices were not symmetric, and moreover, they broke down into a few small vortices that consumed their shear force. Although the combustor was symmetric with respect to the X–Z plane and the velocities of the two jets were equal, the flow near the dome region is shown to be three-dimensional because the curvature in the curved combustor inlet induced secondary flows, which break down into multiple vortices, and complex turbulent characteristics.[6,15,16]

Inlet jets impinged on each other and then attached to the walls downstream of the inlets. Because the adverse pressure distribution was formed near the wall behind the inlet, reverse flow regions

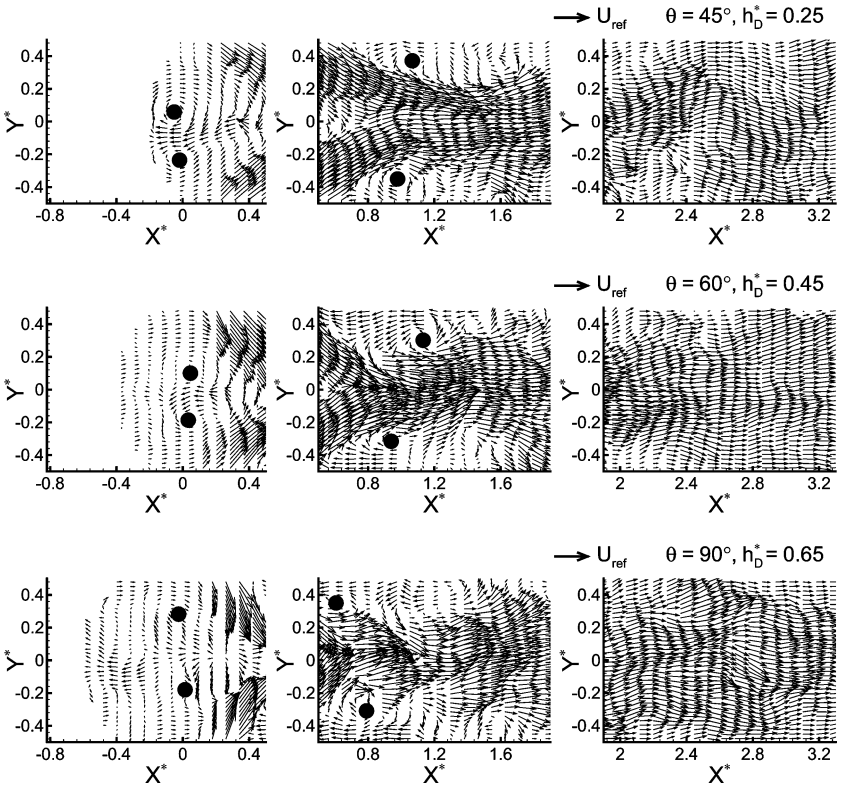

Fig. 3 Instantaneous velocity vector plots.

occurred. The regions consisted of large-scale and small-scale vortices. These vortices interacted violently with the jets and were shown generally by $X^* = 1.8$ as illustrated in Fig. 3. In the downstream direction of $X^* = 2.0$, those vortices were not found anymore. Like the flow in the dome region, the flow downstream of the inlet was believed to be three-dimensional.

Nosseir and Behar[6] found that part of one jet was deflected into the dome and a moment later it was deflected out while the other jet was deflected in. They concluded that the oscillation of each jet into the dome was almost periodic and out of phase with the oscillation of the other jet. Hence, to examine the change of the flowfield with time, instantaneous two-dimensional velocities and vorticity field in the case of $\theta = 60$ deg and $h_D^* = 0.45$ are presented in Fig. 4. The two jets in Fig. 4a are seen to be symmetric. However, a moment later the impinging jet moved up (Fig. 4b) and then it moved down again (Fig. 4c). The results confirmed that the flowfield might change periodically with the oscillation of the two jets.

B. Mean Velocity Characteristics

Figures 5 and 6 show the mean velocity vector plots in the upper half and streamlines and vorticity fields in the lower half. In contrast to the instantaneous flowfields, small-scale vortices were not found, but only large-scale vortices existed near the dome and the walls. Generally, a pair of counter-rotating vortices (the PRZ) appeared between the dome and the impinging point, and a pair of counter-rotating vortices (the SRZ) were generated near each wall downstream of the inlet.

Flowfields with inlet angle that varied at the same dome height ($h_D^* = 0.45$) are presented in Fig. 5, where the mean velocity vectors are 66% skipped from the full vector maps. As reported by Liou and Wu,[8] the flow out of the inlet was not uniform due to the separation in the curved inlet duct. Flow speed in the front edge of the inlet was, therefore, much higher than that in the behind edge. Mean flow velocities in the PRZ and SRZ were much smaller than the flow speed of the inlet jet so that such recirculation zones could act as a flame stabilization region. As the inlet angle increased, the

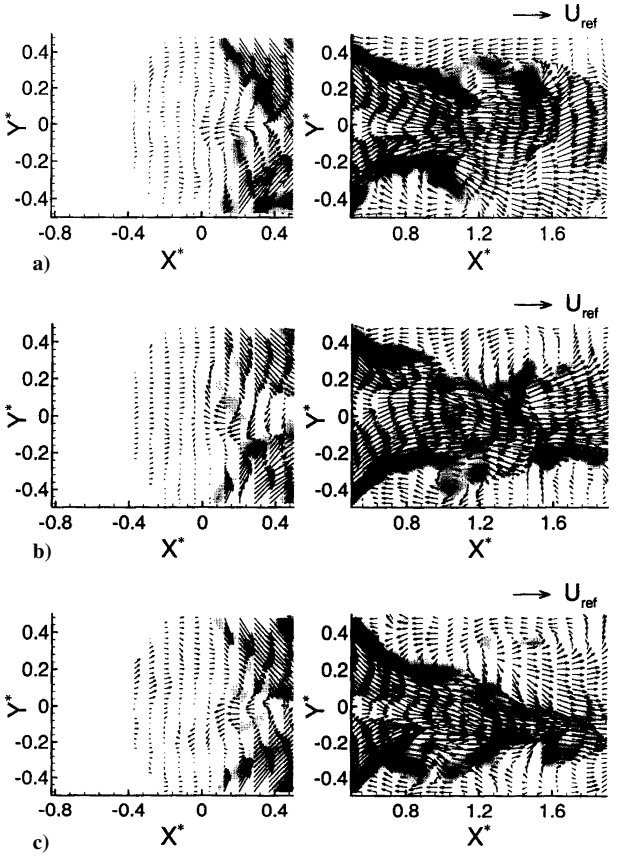

Fig. 4 Instantaneous velocity vector plots and vorticity fields with time in the case of $\theta = 60$ deg and $h_D^* = 0.45$: a) at $t = T$, b) at $t = T + \tau_1$, and c) at $t = T + \tau_2$. T : any reference time; τ_1, τ_2: delay time.

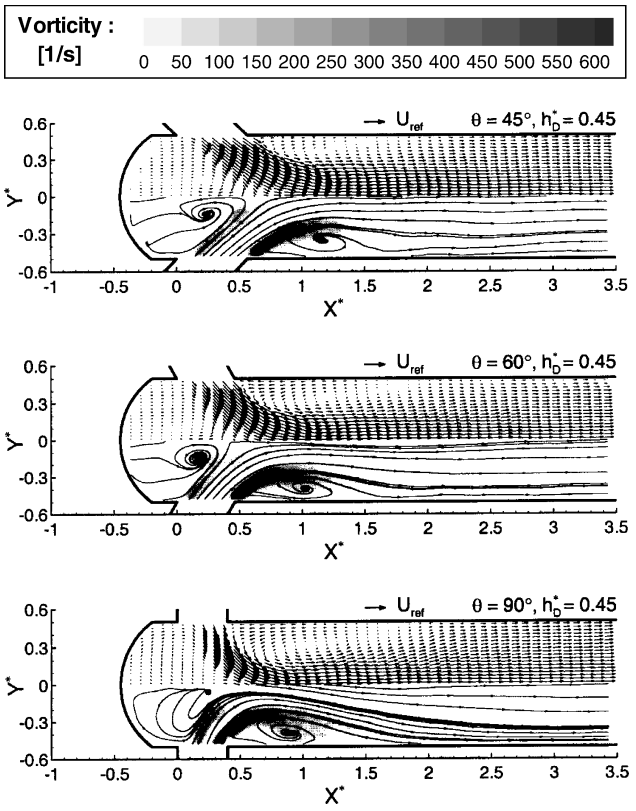

Fig. 5 Mean velocity vector plots and streamlines/vorticity fields with the inlet angle.

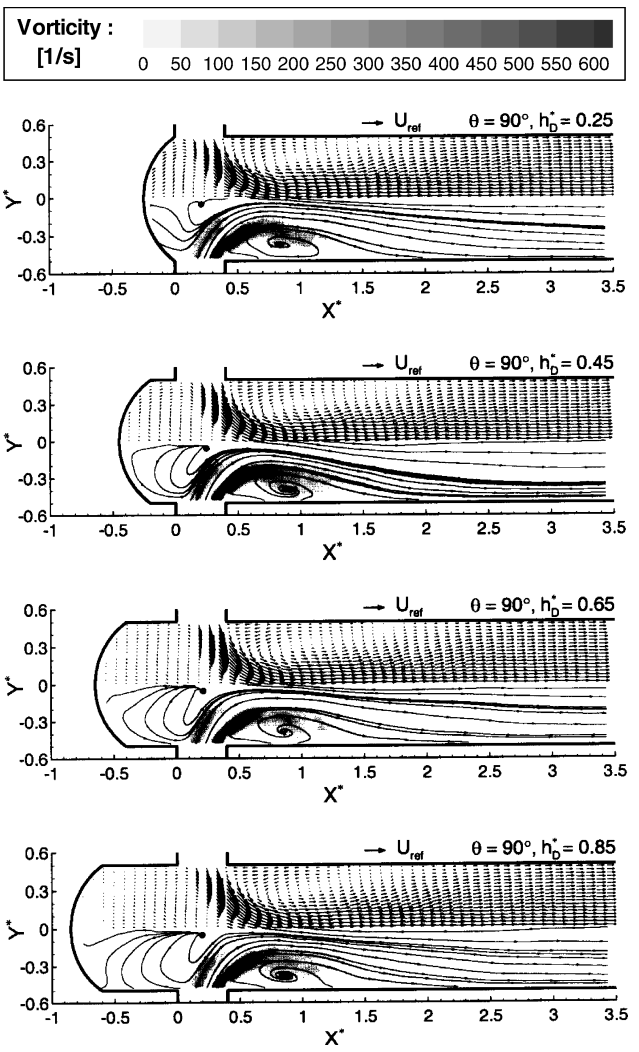

Fig. 6 Mean velocity vector plots and streamlines/vorticity fields with the dome height.

impinging point of two inlet jets moved upstream. Hence, primary reverse flow in the case of $\theta = 45$ deg did not reach the dome end, whereas primary reverse flow in the case of $\theta = 90$ deg reached the dome end.

According to previous research,[8] the SRZ in the three-dimensional circular chamber existed when the dump angle was equal to or larger than 75 deg. However, the present result in the two-dimensional chamber showed that the SRZ took place even in the case of $\theta = 45$ deg. This is believed to be due to the different flow space. As the flow proceeded downstream of the inlet, the maximum axial velocity points approached the centerline and the flow developed initially with a bell-shaped velocity profile and then became uniform.[11]

Flowfields with dome height that varied at the same inlet angle ($\theta = 90$ deg) are presented in Fig. 6. In the case of $h_D^* = 0.25$, the primary reverse-flow region generated near the dome was much smaller than the others because there was not enough space for the reverse-flow. As the dome height increased, the reverse-flow region became broader. However, in the case of very large dome height ($h_D^* = 0.85$), the reverse-flow region did not increase any more. The flowfield downstream of the inlet was not significantly affected by the dome height.

From the vorticity fields ($\omega_z = \partial V/\partial X - \partial U/\partial Y$) in Figs. 5 and 6, it was interesting to find that the high-vorticity region was near the shear layer, which took place in the boundary between the impinging jet and the reverse flow. The mean vorticity fields tended to induce fresh flow toward the vortex core, and the flow might experience fine-scale mixing brought about by vorticity fluctuation as shown in Fig. 4.[6]

The longitudinal components (U) of the centerline velocities are shown in Fig. 7 as functions of the inlet angle and the dome height. It is worth noting that the U profiles had almost the same trend regardless of the dome heights, except for the case when $\theta = 90$ deg. At $\theta = 60$ deg, the values of U/U_{ref} in the PRZ had a similar negative region ($0 < X^* < 0.4$) and the values downstream of the inlet were almost the same. At $\theta = 90$ deg, however, the values in the PRZ had a larger negative region with the dome height increased. Particularly, in the case of $h_D^* = 0.25$, the negative values of U/U_{ref} were found in a very narrow region, because there was not enough space for the reverse flow. Similarly, for $\theta = 90$ deg, the values downstream of the inlet were almost the same regardless of the dome height.

Unlike the dome height, the inlet angle affected the flowfield significantly. The impinging stagnation point, which had $U = 0$ and $V = 0$, and the reverse flow region in the PRZ were generated further upstream as the inlet angle increased; for 45-, 60-, and 90-deg inlet angles at $h_D^* = 0.45$, the stagnation points were found to be at $X^* = 0.59$, 0.41, and 0.25, respectively. Liou et al.[9] reported that the stagnation points could be expressed with the equation $X^* = 0.5 \times \cot\theta$, where θ represented the inlet angle. Consequently, the stagnation points were calculated to be at $X^* = 0.5$, 0.29, and 0 for $\theta = 45$, 60, and 90 deg, respectively. A comparison of the calculated stagnation points with the measured data revealed that these values were underestimated. It is believed that the equation $X^* = 0.5 \times \cot\theta$ does not assume the existence of a separation in the curved inlet duct. However, as the inlet angle decreases, the difference between the calculated value and the measured value becomes smaller. It is thought that for a smaller inlet angle, the effect of the separation in the curved inlet duct decreases so that the difference between the values becomes smaller. Considering the effect of the separation and adding a correction constant, Liou et al.[9] proposed the modified analytical equation $X^* = 0.5 \times \cot\theta + 0.1$. From this equation, the calculated stagnation points were at $X^* = 0.60$, 0.39, and 0.1. The calculated values when $\theta = 45$ and 60 deg showed good agreement with the measured values. However, the calculated value when $\theta = 90$ deg was still underestimated. Since the degree of

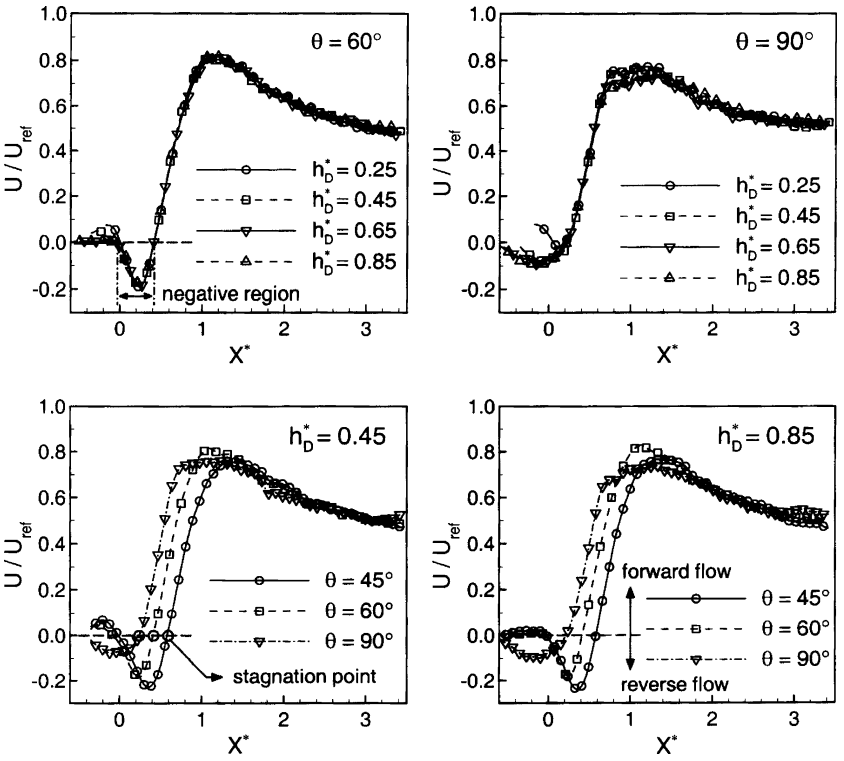

Fig. 7 Longitudinal components of the centerline velocities with the inlet angle and the dome height.

separation in the curved inlet duct varied with the inlet angle, therefore, a correction constant larger than 0.1 should be considered for $\theta = 90$ deg.

Even though the longitudinal directional momentum of the jets at $\theta = 45$ deg was greater than that at $\theta = 60$ deg, the maximum value of the centerline velocities existed at $\theta = 60$ deg, as shown in Figs. 7c and 7d. The reason is believed to be that the height of the SRZ at $\theta = 60$ deg was greater than that at $\theta = 45$ deg. Hence, the area that the impinging flow could pass through became smaller at $\theta = 60$ deg compared to $\theta = 45$ deg. It is interesting to note that the minimum value in the centerline velocities was at $\theta = 45$ deg. It is believed that as the inlet angle increased, the two-dimensional size of the reverse flow increased so that the minimum value in the centerline increased.

C. Recirculation Zones

Figure 8 shows the effects of the inlet angle and the dome height on the SRZ, where the length and the height were obtained by averaging the sizes of the upper and lower SRZ. The length of the SRZ was defined as the length between the points with $U = 0$ at the wall and the height of the SRZ as the length between the point with $U = 0$ and $V = 0$ (recirculation core) and the wall as shown in Fig. 8a. As the inlet angle increased, the height of the SRZ increased almost linearly regardless of the dome height. However, the length of the SRZ generally had a maximum value at $\theta = 60$ deg. From the experimental results, the height of the SRZ normalized by the combustor height could be expressed approximately as

$$H_{\mathrm{SRZ}}/H = 0.180 \sin\theta + 0.023 \tag{1}$$

Because the inlet angle controlled the direction of the flow into the combustor from the curved inlet and the impinging point of two inlet jets, it affected the size of the SRZ significantly, so that the height of the SRZ was varied almost linearly with the inlet angle as shown in Fig. 8b. However, the length of the SRZ did not increase any more in the case $\theta > 60$ deg because the flow in the combustor was confined and the impinging point of two inlet jets went upward with the increase of the inlet angle. On the contrary, the dome height had little effect on the size of the SRZ because the dome height physically had little relation to the flow downstream of the inlet duct.

The fraction of the inlet mass-flow rate that is transported into the recirculation zones may have an important effect on the fluid mixing and the flame stability inside a combustor.[9,13,17,18] The maximum reverse mass-flow rates normalized by the total inlet mass-flow rate are presented in Fig. 9 as functions of the inlet angle and the dome height. The reverse mass-flow rates were calculated by integrating the vectors in the reverse flow region across the longitudinal direction. The maximum reverse mass-flow rate in each recirculation zone was chosen as the maximum value among the integrated values at every longitudinal position. The maximum reverse mass-flow rates in the SRZ were obtained by summing the values in upper SRZ and in lower SRZ. As shown in Fig. 9a, the maximum mass-flow rate in the PRZ increased with the inlet angle. Fig. 9a points out that the dome height at $\theta = 45$ deg did not affect the reverse mass-flow rate significantly, but the dome height $h_D^* = 0.25$ at $\theta = 60$ deg and $\theta = 90$ deg limited the reverse mass-flow rate so that the size of h_D^* needed to be greater than 0.25 for enough reverse mass-flow rates. Except for the case of $h_D^* = 0.25$, the maximum mass flow rate in the PRZ could be approximately obtained as

$$\dot{m}_{\mathrm{max,PRZ}}/\dot{m}_{\mathrm{in}} = 0.147 \sin\theta - 0.041 \tag{2}$$

The values in the SRZ increased as the inlet angle was varied from $\theta = 45$ deg to $\theta = 60$ deg as shown in Fig. 9b. However, the values between $\theta = 60$ deg and $\theta = 90$ deg showed little difference except for $h_D^* = 0.25$. The values in the SRZ were equivalent to those in the PRZ so that the SRZ is believed to be as important as the PRZ for flame stabilization.

According to Shahaf et al.[17] and Kennedy,[18] the fraction of the inlet mass flow rate that is transported into the head region may have an important effect on the fluid mixing and the flame stability inside a combustor. Liou et al.[9] studied the relation between the mass flow rate into the head region and the optimum dome height. They found that the presence of a peak $\dot{m}_{ri}/\dot{m}_{\mathrm{in}}$ was due to the fact that only for a certain optimal head height the head vortex

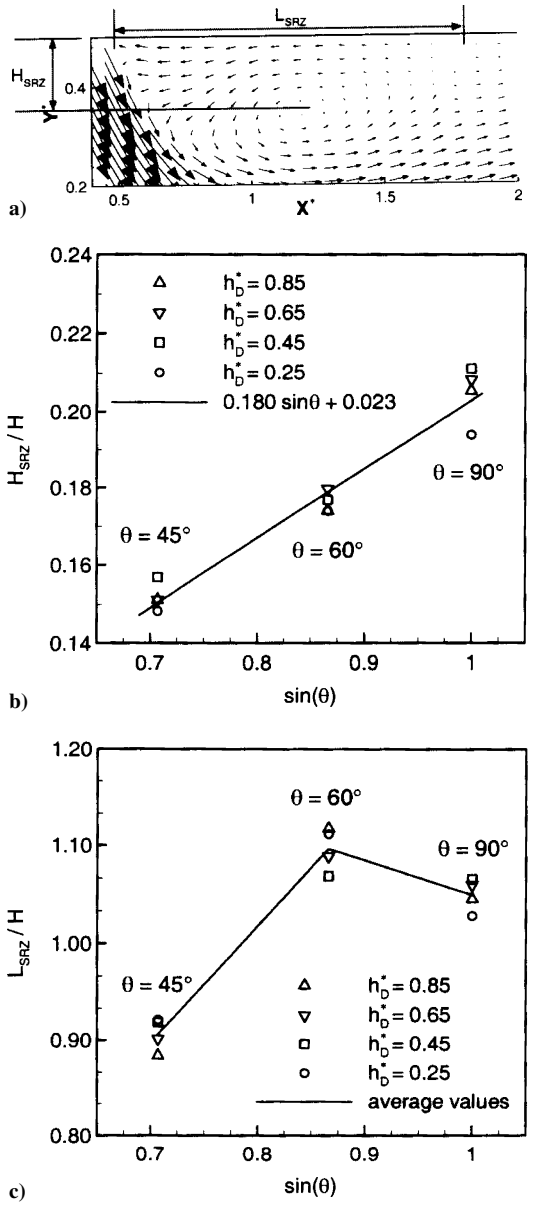

Fig. 8 Effects of the inlet angle and the dome height on SRZ: a) definition of H_{SRZ} and L_{SRZ}; b) height of SRZ; c) length of SRZ.

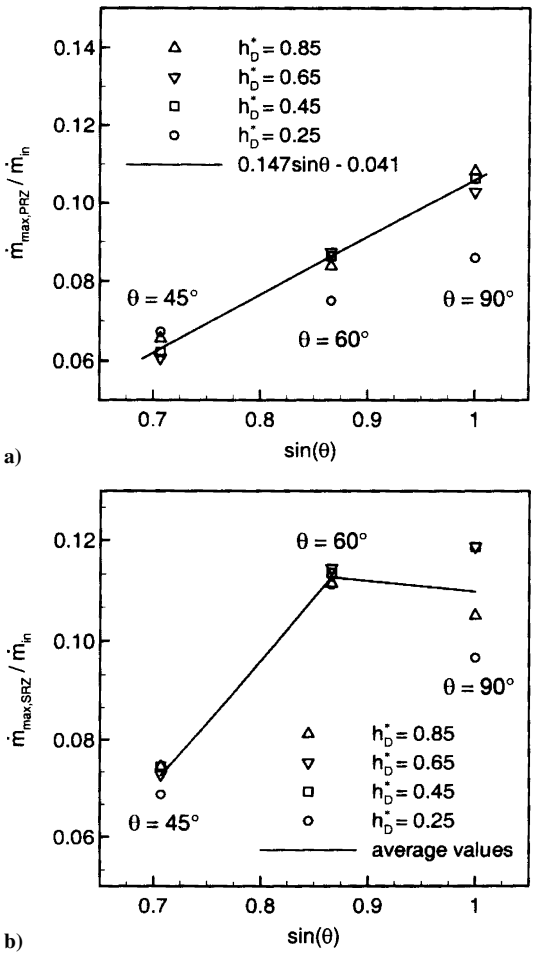

Fig. 9 Effects of the inlet angle and the dome height on the maximum reverse mass flow rate in the recirculation zones: a) PRZ; b) SRZ.

tended to form a smooth circle that could be most easily driven by the inlet jet. They also stated that the existence of an optimal head height for the maximum $\dot{m}_{ri}/\dot{m}_{\text{in}}$, shown by their cold-flow study, paralleled the existence of an optimal head height for the best flame blowoff performance found experimentally by Choudhury[19] and for the best combustion efficiency predicted computationally by Vanka et al.[20]

As shown in Fig. 9, for $\theta = 45$ deg, $\dot{m}_{\text{max,PRZ}}/\dot{m}_{\text{in}}$ and $\dot{m}_{\text{max,SRZ}}/\dot{m}_{\text{in}}$ were not significantly dependent on dome height. For $\theta = 60$ deg, $\dot{m}_{\text{max,PRZ}}/\dot{m}_{\text{in}}$ and $\dot{m}_{\text{max,SRZ}}/\dot{m}_{\text{in}}$ did not increase in case of $h_D^* > 0.45$. For $\theta = 90$ deg, $\dot{m}_{\text{max,PRZ}}/\dot{m}_{\text{in}}$ and $\dot{m}_{\text{max,SRZ}}/\dot{m}_{\text{in}}$ had similar values between $h_D^* = 0.45$ and $h_D^* = 0.65$. However, as shown in Fig. 6, the primary recirculation zone at $h_D^* = 0.65$ was believed to be a little larger than that at $h_D^* = 0.45$. As the dome height increases, the combustor may become heavy. Therefore, the optimum dome height was determined as the minimum dome height that maximized the values of $\dot{m}_{\text{max,PRZ}}/\dot{m}_{\text{in}}$ and $\dot{m}_{\text{max,SRZ}}/\dot{m}_{\text{in}}$. In the present combustor, the optimum dome heights are believed to be $h_D^* = 0.25$, 0.45, and 0.65 for 45-, 60-, and 90-deg inlet angles, respectively.

IV. Summary

Flow characteristics such as instantaneous velocity fields, mean velocity fields, and recirculation zones in the two-dimensional side-dump combustor with two symmetric inlet ducts were investigated by varying the inlet angle and the dome height. The main findings are as follows:

1) Two pairs of counter-rotating vortices were formed upstream of the impinging point of two inlet jets (the PRZ) and near the wall behind the inlet (the SRZ). Unlike the result for the mean flowfield, these vortices were not symmetric. Moreover, they broke down into a few small-scale vortices consuming their shear force. It was found that the flowfield might change periodically with the oscillation of two jets.

2) The longitudinal components of the centerline velocities at the same inlet angle had almost the same trend regardless of the dome height. The stagnation points were found to be at $X^* = 0.59$, 0.41, and 0.25 for 45-, 60-, and 90-deg inlet angles, respectively. These values were a little different from the values calculated by the analytical equation proposed by Liou et al.[9] because the degree of separation in the curved inlet duct varied with the inlet angle.

3) The inlet angle affected the size of the SRZ significantly; the height of the SRZ was almost linear with the inlet angle. However, the dome height had little effects on the size of the SRZ. The maximum reverse mass-flow rate, which was transported into the PRZ, increased with the inlet angle. The values of the maximum reverse mass-flow rate in the SRZ were equivalent to those in the PRZ, so the SRZ is believed to be as important as the PRZ for flame stabilization.

4) From the viewpoint of $\dot{m}_{\text{max,PRZ}}/\dot{m}_{\text{in}}$ and $\dot{m}_{\text{max,SRZ}}/\dot{m}_{\text{in}}$ on the mean flowfield, there was an optimum dome height for each inlet angle. In the present combustor, the optimum dome heights are believed to be $h_D^* = 0.25$, $h_D^* = 0.45$, and $h_D^* = 0.65$ for 45-, 60-, and 90-deg inlet angles, respectively.

Acknowledgments

This work was supported by Grant M1-0104-00-0058 from the National Research Laboratory program of the KISTEP (Korea Institute of Science & Technology Evaluation and Planning). This support is gratefully acknowledged.

References

[1]Drewry, J. E., "Fluid Dynamic Characterization of Sudden-Expansion Ramjet Combustor Flowfields," *AIAA Journal*, Vol. 16, No. 4, 1978, pp. 313–319.

[2]Edelman, R. B., Harsha, P. T., and Schmotolocha, S., "Modeling Techniques for the Analysis of Ramjet Combustion Processes," AIAA Paper 80-1190, June–July 1980.

[3]Yang, B. T., and Yu, M. H., "The Flowfield in a Suddenly Enlarged Combustion Chamber," *AIAA Journal*, Vol. 21, No. 1, 1983, pp. 92–97.

[4]Webster, F. F., "Liquid Fueled Integral Rocket/Ramjet Technology Review," AIAA Paper 78-1108, July 1978.

[5]Stull, F. D., Craig, R. R, Streby, G. D., and Vanka, S. P., "Investigation of a Dual Inlet Side-Dump Combustor Using Liquid Fuel Injection," *Journal of Propulsion and Power*, Vol. 1, No. 1, 1985, pp. 83–88.

[6]Nosseir, N. S., and Behar, S., "Characteristics of Jet Impingement in a Side-Dump Combustor," *AIAA Journal*, Vol. 24, No. 11, 1986, pp. 1752–1757.

[7]Nosseir, N. S., Peled, U., and Hildebrand, G., "Pressure Field Generated by Jet-on-Jet Impingement," *AIAA Journal*, Vol. 25, No. 10, 1987, pp. 1312–1317.

[8]Liou, T. M., and Wu, S. M., "Flowfield in a Dual-Inlet Side-Dump Combustor," *Journal of Propulsion and Power*, Vol. 4, No. 1, 1988, pp. 53–60.

[9]Liou, T. M., Hwang, Y. H., and Wu, S. M., "The Three-Dimensional Jet–Jet Impingement Flow in a Closed-End Cylinderical Duct," *Journal of Fluids Engineering*, Vol. 112, June 1990, pp. 171–178.

[10]Liou, T. M., Hwang, Y. H., and Chen, L., "Prediction of Confined Three-Dimensional Impinging Flows with Various Turbulence Models," *Journal of Fluids Engineering*, Vol. 114, June 1992, pp. 220–230.

[11]Manjunath, A., Gowda, B. H. L., and Natarajan, R., "Studies on the Mixing of Two Non-axial Plane Jets in a Confined Passage: Mean Flow Characteristics," *Experiments in Fluids*, Vol. 11, No. 1, 1991, pp. 17–24.

[12]Manjunath, A., Gowda, B. H. L., and Natarajan, R., "Studies on the Mixing of Two Non-axial Plane Jets in a Confined Passage—Turbulence Characteristics," *Experiments in Fluids*, Vol. 13, No. 2–3, 1992, pp. 147–154.

[13]Yen, R. H., and Ko, T. H., "Effects of Side-Inlet Angle in a Three-Dimensional Side-Dump Combustor," *Journal of Propulsion and Power*, Vol. 9, No. 5, 1993, pp. 686–693.

[14]Hart, D. P., "The Elimination of Correlation Errors in PIV Processing," *Proceedings of the 9th International Symposium on Application of Laser Techniques to Fluid Mechanics*, July 1998.

[15]Liou, T. M., and Liao, C. C., "Flows in a Curved Combustor Inlet with and without a Guide Vane," *Journal of Propulsion and Power*, Vol. 11, No. 3, 1995, pp. 464–472.

[16]Iacovides, H., Launder, B. E., Loizou, P. A., and Zhao, H. H., "Turbulent Boundary-Layer Development around a Square-Sectioned U-Bend: Measurements and Computation," *Journal of Fluids Engineering*, Vol. 112, Dec. 1990, pp. 409–415.

[17]Shahaf, M., Goldman, Y., and Greenberg, J. B., "An Investigation of Impinging Jets in Flow with Sudden Expansion," *Proceedings of the 22nd Israel Annual Conference on Aviation and Astronautics*, Israel Ministry of Transport, Tel Aviv, 1980, pp. 100–106.

[18]Kennedy, J. B., "Ramburner Flow Visualization Studies," *Proceedings of 11th JANNAF Combustion Meeting*, Vol. II, CPIA Pub., Columbia, MD, 1974, pp. 415–440.

[19]Choudhury, P. R., "Characterization of a Side Dump Gas Generator Ramjet," AIAA Paper 82-1258, 1982.

[20]Vanka, S. P., Craig, R. R., and Stull, F. D., "Mixing, Chemical Reaction and Flow Field Development in Ducted Rockets," AIAA Paper 85-1271, 1985.